Static and fatigue strength of laser-textured adhesive-bonded polyamide 66 (PA 66) joints

Static and fatigue strength of laser-textured adhesive-bonded polyamide 66 (PA 66) joints

Adrian H.A. LUTEY, Fabrizio MORONI, Claudio FAVI, Núria BOIX RODRIGUEZ

PII: S0143-7496(22)00072-0

DOI: https://doi.org/10.1016/j.ijadhadh.2022.103155

Reference: JAAD 103155

To appear in: *International Journal of Adhesion and Adhesives*

Received Date: 3 February 2022

Accepted Date: 27 March 2022

Please cite this article as: LUTEY AHA, MORONI F, FAVI C, BOIX RODRIGUEZ N, Static and fatigue strength of laser-textured adhesive-bonded polyamide 66 (PA 66) joints, *International Journal of Adhesion and Adhesives*, https://doi.org/10.1016/j.ijadhadh.2022.103155.

Static and fatigue strength of laser-textured adhesive-bonded polyamide 66 (PA 66) joints

Adrian H.A. LUTEY*, Fabrizio MORONI, Claudio FAVI, Núria BOIX RODRIGUEZ
Dipartimento di Ingegneria e Architettura, Università di Parma, Parco Area delle Scienze 181/A, 43124 Parma, Italy
*Corresponding author: Tel: +39 0521 906029, Fax: +39 0521 905924, email: adrian.lutey@unipr.it

Nanosecond pulsed laser texturing has been performed as surface preparation for adhesive-bonded polyamide 66 (PA 66) joints. A Design-of-Experiments approach was firstly applied for optimization of laser parameters in terms of static joint strength, after which the fatigue strength of the best performing joints was determined. Quasi static and fatigue lap shear tests were performed on joints bonded with Teroson PU 9225. Laser texturing of PA 66 was found to be far less sensitive to heat accumulation in the hatch direction than in the laser scanning direction. Static average shear strength was generally found to increase with laser energy dose up to approximately 8-20 J/cm^2, while no correlation was observed between the microscale surface roughness and static strength for low values of the former (S_a < 2 µm). A shear strength of 11.60 MPa was achieved with a parallel-line scanning strategy and an average laser power of 3 W, hatch spacing of 50 µm and scanning velocity of 700 mm/s, representing a three-fold increase over standard primed joints. Laser-textured joints prepared with the same parameters exceeded the fatigue performance of atmospheric pressure plasma, mechanical abrasion and primer pre-treatments at both high and low maximum average cyclic shear stress, implying that laser texturing is an appropriate solution for improving bonding at high cyclic shear stress and prolonging the crack propagation phase at low cyclic shear stress.

Keywords: Laser Texturing; Adhesives; Surface Preparation; Polymer; Polyamide; Fatigue

1 INTRODUCTION

Engineering polymers find widespread use in products ranging from medical devices to aerospace components. Their uptake is driven primarily by their low density and cost, good corrosion resistance and ease of manufacturing. Polyamide 66 (PA 66) is an engineering polymer characterized by high strength and stiffness, finding use in components such as tanks, hinges, piping and lightweight structural elements. PA 66 is a good alternative to metal when reinforced with glass fibers, making it suitable for applications in the automotive field where high strength and low weight are of primary importance, as well as resistance to oscillating stresses and vibration. In an extensive review of polymer joining techniques, Silva et al. [1] note that welding, mechanical fasteners and adhesive bonding all play a key role in enabling the economical manufacturing of complex polymer components at large scale. In relation to adhesive bonding, reliable joining of PA 66 is a complex task due to its low surface energy and wettability. Surface preparation of polymers is usually required to achieve acceptable bonding between the adhesive and substrate by inducing changes in surface chemistry and/or morphology. ASTM D2093 [2] indicates preparation with a sulfuric acid-dichromate solution or mechanical abrasion for preparation of adhesive-bonded polymer joints. Ebnesajjad [3] provides comprehensive material-specific guidelines that also include plasma and oxidizing flame treatments. Lutey and Moroni [4] recently demonstrated nanosecond pulsed laser irradiation as an alternative for the preparation of polymer adhesive-bonded joints. Performed with a common laser-marking setup, this technology is precise, versatile and fast, with excellent scalability and no requirements for chemical handling, thus providing a number of advantages over other surface preparation methods.

The interaction between a focused laser beam and a polymeric substrate depends on the wavelength and intensity of the laser beam, as well as the optical and thermal properties of the target material. Cutting and welding of polymers has historically been performed with CO_2 lasers emitting at a wavelength of 10,6 µm or ultraviolet lasers emitting at wavelengths below 400 nm, where optical absorption in organic materials is strong. Lippert [5] notes that material transformation takes place via photothermal pathways in the former case, while both photothermal and photochemical phenomena may take place during irradiation with an ultraviolet laser. As discussed by Kagan et al. [6] in relation to laser welding of polyamides, most pure polymers are largely transparent at 1064 nm, the emission wavelength of Yb and Nd-doped lasers widely employed for industrial laser marking and engraving of metals; however, the presence of fiber reinforcement, fillers, modifiers and pigments can lead to strong absorption and localized temperature rise. The precise optical properties of pigmented polymers at 1064 nm are often unknown, requiring systematic experiments to be performed for a given application. Nonetheless, the benefits of operating at this wavelength in terms of cost and power scalability justify its use where a stable process can be achieved. With sufficient optical absorption, the low thermal conductivity of most polymers leads to rapid heating and phase transformation with relatively limited power density, which in turn leads to modification of the morphology via complete or partial ejection of material, as well as direct or thermally induced changes to surface chemistry. The use of nanosecond laser pulses for

ablation of polymers, as discussed at length by Ravi-Kumar et al. [7], further limits thermal conduction and can therefore be employed to induce precise material transformation and surface texturing while also limiting heat accumulation and macroscopic melting effects beyond the irradiated region.

In a previous study by Lutey and Moroni [4], laser-texturing of polyethylene (PE) substrates was performed to achieve surface protrusions less than 100 µm in diameter resulting from partial ejection of molten material during laser exposure. These surface features were shown to improve the static shear strength of PE lap joints bonded with Teroson 9399 by up to 79% compared to standard primed joints, from 0.83 MPa to 1.49 MPa. Lap shear strength was found to increase with laser energy dose up to the onset of macroscopic melting, while maximum joint strength corresponded to values of surface roughness within the range Sa = 1.5 – 3.5 µm. Several studies have investigated the use of surface treatments such as atmospheric-pressure plasma and vacuum UV exposure to improve the static strength of adhesive-bonded engineering and reinforced polymer joints. Schäfer et al. [8] found that plasma treatment of carbon fiber reinforced polyamide 6 (PA 6) increased the surface energy, oxygen content and number of functional groups, achieving a lap shear strength of up to 20 MPa with a two-component polyurethane adhesive compared to 7 MPa with cleaned surfaces. The authors also found that flattening of the nanoscale surface topography due to onset of melting with high intensity plasma treatment was detrimental to joint strength. Kłonica et al. [9] found that ozone treatment also increased the surface energy of PA 6 by up to 20%, achieving a lap shear strength of up to approximately 3.2 MPa with Hysol 9466 following 10 g/m^3 ozone exposure for 5 minutes, compared to approximately 2.3 MPa with no ozone treatment. Mandolfino et al. [10] performed air low-pressure plasma treatment on PA 6 and PA 66, demonstrating a reduction in the water contact angle from 50° on untreated polymer to as low as 2° due to the presence of oxidized degradation products. Lap shear strength with DP8810 bi-component acrylic adhesive was increased from 0.60 MPa for PA 6 and 1.65 MPa for PA 66 with cleaned and abraded surfaces to 4.07 MPa and 6.47 MPa following plasma treatment. More recently, Arikan et al. [11] investigated oxygen low-pressure plasma and vacuum UV pretreatment of polyetheretherketone, polyetherimide, polyethersulfone and RTM6 epoxy resin, performing extensive analysis in terms of surface chemistry, wettability and topography. The authors determined the presence of low molecular weight oxidized material following surface treatment; however, they found that upon washing this material was essentially removed, implying that changes in chemistry and wettability were of lesser influence than molecular-scale topography.

In relation to the fatigue performance of polymer adhesive-bonded joints, Musiari and Moroni [12] recently compared degreasing, mechanical abrasion and atmospheric pressure plasma pretreatments, as well as combinations of these processes, for PA 66 joints bonded with Teroson PU 9225 subject to static and cyclic shear loading in a lap joint configuration. This approach decoupled the effects of chemistry and morphology, with plasma treatment alone achieving highest static strength (9.46 MPa), but a combination of abrasion and plasma treatment achieving best fatigue performance. In relation to plasma treatment, Pappas et al. [13] discussed how the driving factor improving bonding of polyamide is the formation of hydroxylic and carboxylic groups, leading to increases in surface oxygen content and wettability. Quaresimin and Ricotta [14] analyzed the fatigue damage evolution of carbon/epoxy laminates bonded with epoxy, finding that the crack nucleation phase accounted for 20-70% of joint life. Shenoy et al. [15] used the backface strain measurement technique to demonstrate that crack propagation dominates at high load amplitude while crack initiation dominates at low load amplitude. Within this context, the results presented by Musiari and Moroni [12] highlight the separate roles of adhesion and morphology in improving the fatigue performance of PA 66 adhesive-bonded joints, as increased oxygen content and wettability induced by plasma treatment improved bonding under static and high-amplitude cyclic loading, while increased surface roughness induced by abrasion prolonged the crack propagation phase under low-amplitude cyclic loading.

Laser irradiation has the potential to achieve changes to both adhesion and morphology, representing a novel approach for improving the static and fatigue performance of polymer adhesive-bonded joints. The goal of the present work was therefore to investigate the static and fatigue strength of laser-textured adhesive-bonded PA 66 joints with the aim of comparing this approach to existing surface treatments and determining potential implications for optimization of process parameters. Nanosecond pulsed laser texturing was applied for the preparation of PA 66 adhesive-bonded joints to optimize both static and fatigue performance in a single-step process. A Design-of-Experiments (DoE) was firstly developed for the selection of laser parameters including average power, scanning velocity, hatch spacing and scanning strategy. This approach was applied to optimize laser parameters in terms of static joint strength without requiring detailed knowledge of the optical properties of the substrate. Focus was then shifted to the fatigue strength of the best performing joints, which were compared to joints prepared with primer, abrasion and atmospheric pressure plasma pretreatments. Further to applying laser irradiation to a new adhesive-substrate combination, expanding the range of possible applications for this surface treatment, comparison of results obtained with different surface pretreatments

under the same conditions allowed improvements in the fatigue performance of laser-textured polymer adhesive-bonded joints to be quantified for the same adhesive-substrate combination. Nanosecond pulsed laser irradiation was found to greatly improve mechanical performance at both high and low cyclic shear stress compared to all other tested surface pretreatments.

2 MATERIALS AND METHODS

2.1 Samples and adhesive

PA 66 plates with dimensions 100 mm (length) × 25 mm (width) × 6.6 mm (thickness) were bonded together to produce single lap joints in the configuration shown in Fig.1. Joint geometry and testing conditions were in line with ASTM D3163 [16]. The adhesive thickness (t) was set to 0.3 mm while the overlap length (OL) was set to 10 mm for quasi static lap shear tests and 18 mm for fatigue tests to allow subsequent comparison with the fatigue behavior of other joining techniques. The adhesive selected for experiments was Teroson PU 9225, a two component, room temperature curing polyurethane suitable for bonding polymeric components. The adhesive was supplied by Henkel (Milan, IT), while the substrate plates were supplied by Ensinger (Milan, IT). Tables 1 and 2 show the details of each material and the main mechanical properties declared by the respective suppliers.

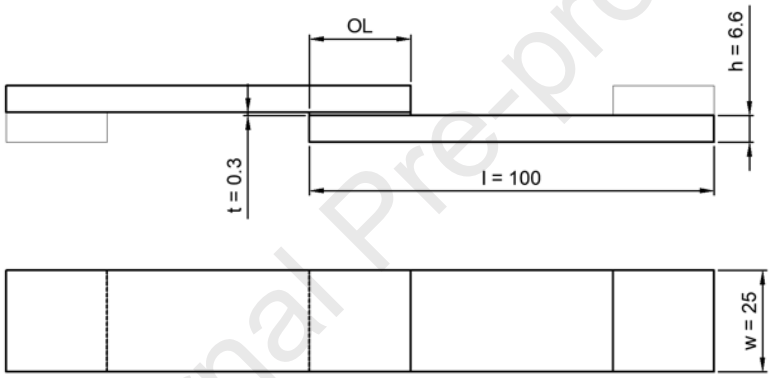

Fig. 1 Single lap joint geometry employed for experiments (dimensions in mm).

Table 1 Material details and main mechanical properties of Teroson PU 9225 adhesive employed for experiments.

Property	**Value**
Technology	Two component polyurethane
Density	1.55 g/cm³
Curing Conditions	5 hrs at 23°C
Shear Strength	approx. 13 MPa
Shore-A Hardness	approx. 90

Table 2 Material details and main mechanical properties of PA 66 employed for experiments.

Property	**Value**
Commercial name	Tacamid 66 MO Black
Additives	<2 w/w % (Black pigment and molybdenum bisulfide)
Density	1.15 g/cm³
Tensile Strength (DIN EN ISO 527-2)	84 MPa
Tensile Elastic Modulus (DIN EN ISO 527-2)	3200 MPa
Tensile Yield Stress (DIN EN ISO 527-2)	83 MPa
Elongation at Break (DIN EN ISO 527-2)	40%

2.2 Laser setup

A nanosecond pulsed fiber laser equipped with a collimator, galvanometric scanning head and f-theta lens was employed for all experiments. The main characteristics of the laser setup are given in Table 3. Although the laser was capable of emitting at an average power of up to 17 W, experiments were limited 6 W due to strong absorption of the laser beam by the target material.

Table 3 Main characteristics of the laser setup utilized for experiments

Parameter	**Value**
Make	LaserPoint
Model	YFL 20P
Wavelength (λ)	1064 nm
Pulse duration (τ)	104 ns
Repetition rate (R)	20 kHz
Average power (P)	1 – 17 W
Pulse energy (E_p)	50 – 850 µJ
Beam quality (M^2)	1.8
Focal length (f)	160 mm
Focused Gaussian spot diameter (d_0)	60 µm
Rayleigh length	1.45 mm
Peak pulse fluence (F)	3.5 – 60.1 J/cm^2
Maximum scanning velocity (v)	2500 mm/s
Working area	100 mm × 100 mm

2.3 Laser texturing

Laser texturing was performed over areas of 25 mm × 15 mm on PA 66 samples, varying the average laser power, P, scanning velocity, v, and lateral hatch distance, h. The textured area was slightly larger than the joint overlap area to ensure that complete coverage was achieved and discontinuities were avoided at edges. Parallel-line (PL) and crossing-line (CL) scanning strategies were employed for experiments. For the PL strategy, the laser beam was scanned over the target surface in a series of equally spaced parallel lines orthogonal to the mechanical load direction. For the CL strategy, a second laser pass was performed with an angular offset of 90°. Schematics of both PL and CL scanning strategies are shown in Fig. 2. For selection of P, v and h, a DoE approach previously applied to PE adhesive-bonded joints by Lutey and Moroni [4] was employed for optimization of static joint strength. A preliminary set of tests was firstly carried out on PA 66 to determine an appropriate laser parameter range over which material modification took place but macroscopic melting was avoided, as the latter had been found to achieve poor adhesion due to the removal of laser-induced surface features. The peak pulse fluence (F) and laser energy dose (E) were calculated as follows:

$$F = \frac{8E_p}{\pi d_0^2} \quad (1)$$

$$E = \frac{P}{vh} \quad (2)$$

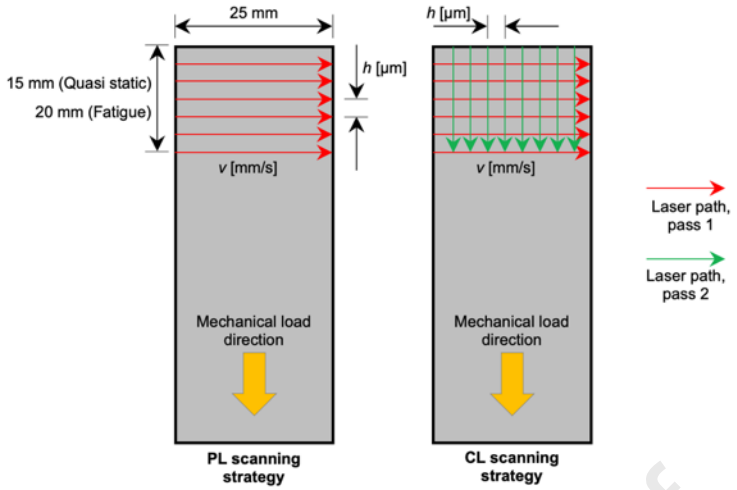

Fig. 2 Schematics of PL and CL laser scanning strategies. Image not to scale.

A first set of experiments was performed for each scanning strategy following a randomized two-level factorial DoE with the levels given in Table 4. Three sample pairs were prepared for all combinations of upper and lower levels within the DoE, while five samples were prepared for the central point. This strategy allowed general trends to be observed based on the gradient of the resulting ANOVA model surfaces. Optimization was then performed with a randomized central composite DoE with the levels given in Table 5. In this case, central values were chosen as the highest value of P and lowest values of v and h from the first set of experiments, as highest joint strength had been achieved with these parameters. Two sample pairs were produced for all combinations of upper and lower levels, as well as axial runs with an axial spacing of 1.68 (see Montgomery et al. [17]), while four samples were prepared for the central point. Use of a randomized central composite DoE in this case allowed a higher-order ANOVA model to be introduced for identification of the maximum joint strength. Similar trends were observed for both PL and CL scanning strategies during the first set of tests, for which the same parameter ranges were employed for both scanning strategies during the optimization phase. ANOVA analyses were performed with the software Design Expert 7.0 (StatEase, Minneapolis USA) [18]. All combinations of process parameters for each set of experiments are given in Tables 8 – 11 in the Appendix.

Table 4 Two-level factorial DoE levels and resulting parameter ranges for first set of experiments. See Tables 8 and 10 in the Appendix for all combinations of process parameters for PL and CL scanning strategies, respectively.

Parameter	**Level #1**	**Center**	**Level #2**
Average power (P)	1 W	2 W	3 W
Scanning velocity (v)	700 mm/s	1400 mm/s	2100 mm/s
Hatch spacing (h)	50 µm	100 µm	150 µm
Peak pulse fluence (F)	3.5 – 10.6 J/cm^2		
Long. pulse spacing	35 – 105 µm		
Lat. pulse spacing	50 – 150 µm		
Total energy dose (E)	0.3 – 17.1 J/cm^2		

Table 5 Central composite DoE levels and resulting parameter ranges for second set of experiments. See Tables 9 and 11 in the Appendix for all combinations of process parameters for PL and CL scanning strategies, respectively.

Parameter	**Level #1**	**Center**	**Level #2**
Average power (P)	2 W	3 W	4 W
Scanning velocity (v)	350 mm/s	700 mm/s	1050 mm/s
Hatch spacing (h)	25 µm	50 µm	75 µm
Peak pulse fluence (F)	7.1 – 14.2 J/cm^2		
Long. pulse spacing	18 – 52 µm		
Lat. pulse spacing	25 – 75 µm		
Total energy dose (E)	2.5 – 107.7 J/cm^2		

Following quasi static lap shear tests, 10 identical sample pairs were produced for subsequent fatigue tests. Laser pretreatment of these specimens was performed with the laser parameters that had achieved the best combination of processing time and joint strength during static tests. A PL scanning strategy was employed over an area of 25 mm × 20 mm with the parameters given in Table 6, as best results had been obtained with this configuration. The textured area was again slightly larger than the joint overlap area to ensure that complete coverage was achieved and discontinuities were avoided at the edges.

Table 6 Laser parameters employed for preparation of fatigue test specimens with PL scanning strategy.

Parameter	Value
Average power (*P*)	3 W
Scanning velocity (*v*)	700 mm/s
Hatch spacing (*h*)	50 µm
Peak pulse fluence (*F*)	10.6 J/cm^2
Long. pulse spacing	35 µm
Lat. pulse spacing	50 µm
Total energy dose (*E*)	8.6 J/cm^2

2.4 Surface topography analysis

The microscale surface topography of all textured samples was analyzed with a Taylor Hobson CCI optical profiler. The instrument was equipped with a 50× objective, providing a vertical resolution of <1 nm and a horizontal resolution of 0.4 µm over an acquisition area of 346 µm × 346 µm. Horizontal stitching was performed in a 2 × 2 configuration to obtain topography maps over a total area of 610 µm × 610 µm. Data processing was performed with Taylor Hobson TalyMap software to level the acquired surface profile, prepare images and quantify the microscale surface roughness (arithmetic mean height, S_a) in line with ISO 25178-2 [19]. The choice of instrument employed for surface profile acquisition was based on the characteristic dimensions of the resulting topography. Surface features yielding best outcomes in terms of static shear strength were several tens of micrometers high and were separated by 35 µm in the laser scanning direction and 50 µm in the lateral direction. These protrusions were clearly identifiable with the optical profiler and could be accurately characterized with this technique. Characterization of the nanoscale surface roughness, found to be of importance for treatments leading to surface features on the nanometer scale [8,11], was excluded in the present work due to the prevalence of microscale surface roughness following laser irradiation within the tested parameter range.

2.5 Adhesive joint production

Prior to bonding, the PA 66 plates were washed and degreased to remove dirt and dust, after which they were subject to laser irradiation. Subsequently, the plates were assembled to create a single lap joint and left at room temperature to cure. A specifically designed jig was used to control the overlap length and adhesive thickness. In order to ensure complete curing of the adhesive, mechanical tests were carried out at least 48 hours after bonding.

Further to the laser-textured specimens, at least three samples were prepared with the following pre-treatments to provide reference values:

- *Untreated*: Substrates were only washed and degreased before bonding. No other treatment was performed.
- *Abrasion*: Once washed and cleaned, the PA 66 plates were abraded with aluminum oxide 320 grit sandpaper in line with guidelines given in ASTM D 2093 [2]. Samples were then wiped with Henkel 7063 cleaner to remove residual abrasive particles, with bonding performed within 10 minutes of treatment.
- *Primer*: Once washed and cleaned, the PA 66 plates were initially abraded as described above and then treated by applying a thin layer of Teroson 150 primer supplied by Henkel (Milan, IT). The primer was left to evaporate for approximately 10 minutes, after which the adhesive was applied.
- *Plasma*: Once washed and cleaned, the PA 66 plates were subject to atmospheric pressure plasma treatment with the procedure described by Moroni et al. [20]. A PlasmaBeam machine supplied by Diener (Diener electronic GmbH & Co. KG, Ebhausen, Germany) was used, equipped with a 2 mm diameter circular nozzle. The nozzle stand-off distance was 5 mm and the translational speed was 100 mm/s, with bonding performed within 10 minutes of treatment.

2.6 Quasi static lap shear tests

Quasi static lap shear tests were carried out in line with ASTM D3163 [16] using an Instron 440 electro-mechanical machine equipped with a 30 kN load cell. Tests were performed at a speed of 1.3 mm/min, with the crosshead displacement and applied load recorded for the entire duration of each test. The maximum value of the load before failure was identified in each case.

2.7 Fatigue tests

Fatigue tests were carried out using a servo-hydraulic MTS 810 testing machine equipped with a 5 kN load cell. Tests were performed in line with ASTM D3166 [21]. Though intended for metal adherends, this standard was employed as no ASTM standard is available for fatigue testing of polymeric bonded joints. Tests were executed under load control by imposing a sinusoidal wave with a load ratio, R, of 0.1 and a frequency of 6 Hz until catastrophic fracture of the specimen took place. The load ratio was imposed according to ASTM D3166, while the loading frequency was selected to shorten the test duration as much as possible while simultaneously avoiding heating of specimens due to cyclic hysteresis. The number of cycles to failure was identified in each test.

3 RESULTS AND DISCUSSION

3.1 Quasi static lap shear tests

3.1.1 Energy dose, average areal roughness and reference treatments

The effects of laser energy dose, E, and microscale surface roughness, S_a, were examined independently prior to analyzing experimental outcomes in terms of individual process parameters. The static average shear strength for all test groups is presented as a function of both parameters in Fig. 3. Shear strength was found to increase with energy dose up to approximately E = 8-20 J/cm^2, after which dispersion of results increased and lower values were obtained. The highest value of average shear strength, 11.64 MPa, was close to the adhesive shear strength declared by the supplier (approximately 13 MPa, Table 1). These outcomes indicate that joint strength was positively associated with laser energy dose up to 20 J/cm^2, after which no further gains were achieved while the risk of large-scale melting and poor joint performance increased. Similar trends were observed for PE in a previous study by Lutey and Moroni [4] up to 17 J/cm^2; however, PA 66 was found to be less sensitive to melting than PE, leading to a larger process parameter window over which consistently high joint strength could be achieved.

No correlation between the microscale surface roughness and static joint strength was observed for low values of the former (S_a < 2 µm). Higher roughness was instead associated with lower dispersion, with consistently high values of shear strength achieved for S_a > 5 µm. While mechanical interlocking may have played a more significant role with higher values of S_a, it should be noted that surface roughness increased with laser energy dose up to the onset of melting, at which point lower roughness resulted due to removal of laser-induced surface features. High values of S_a therefore indicated high energy dose and lack of large-scale melting; criteria associated with, but not necessary for, high joint strength. These outcomes are fundamentally different to trends observed for PE joints bonded with Teroson 9399 [4], where joint strength was positively associated with surface roughness up to S_a = 1.5 – 3 µm, after which joint strength decreased. These differences suggest that changes in microscale morphology play a less important role in relation to static joint strength in the present case, with high values of strength not necessarily associated with specific values of surface roughness. Further investigation into the resulting topography on the nanoscale may be beneficial to further understanding the observed outcomes.

The average shear strength of bonded joints prepared with no treatment, primer, abrasion and atmospheric pressure plasma are reported in Table 7. It can be observed that surface preparation significantly affected joint performance. Amongst the aforementioned treatments, plasma treatment was the most effective; however, the highest value of average shear strength achieved with laser irradiation, 11.64 MPa, was 4.3×, 3.4×, 2.5× and 1.4× as high as the average shear strength achieved with no treatment, primer, abrasion and plasma, respectively. The highest value of shear strength achieved with laser irradiation was 23% higher than that achieved by Musiari and Moroni [12] with plasma treatment in the same configuration (9.46 MPa). The increase compared to untreated/cleaned samples (4.3× as high) was also greater than that achieved by Schäfer et al. [8] with plasma treatment of carbon fiber reinforced PA 6 bonded with a two-component polyurethane adhesive (2.9× as high, from 7 MPa to 20 MPa), and that achieved by Kłonica et al. [9] with ozone treatment of PA 6 bonded with Hysol 9466 (1.4× as high, from 2.3 MPa to 3.2 MPa). Mandolfino et al. [13] instead achieved greater increases compared to cleaned and abraded samples with air low-pressure plasma treatment of PA 6 and PA 66 bonded with DP8810 bi-component acrylic adhesive (6.8× as high for PA 6, from 0.60 MPa to 4.07 MPa, and 3.9× as high for PA 66, from 1.65 MPa to 6.47 MPa).

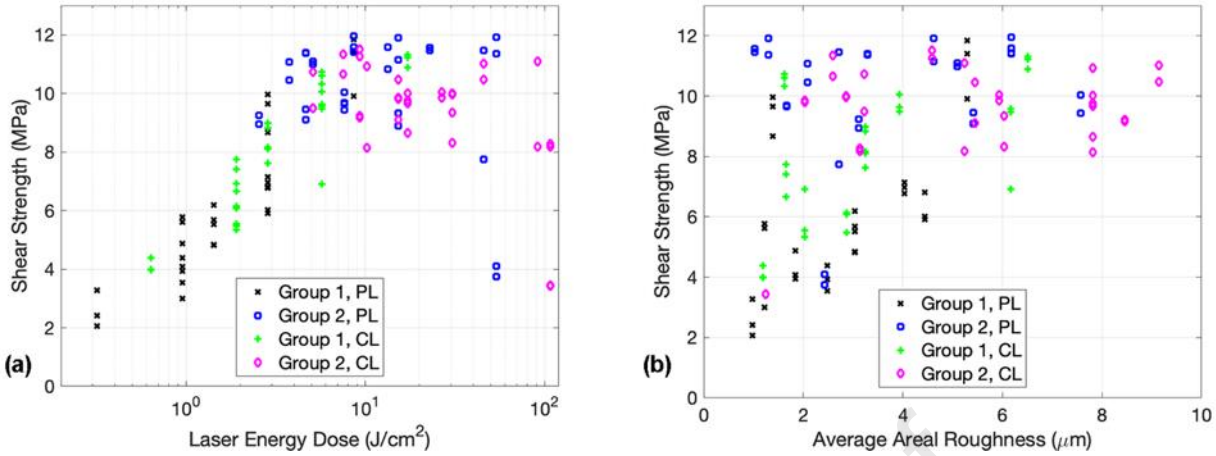

Fig. 3 Average shear strength of adhesive-bonded joints as a function of (a) laser energy dose and (b) average areal roughness.

Table 7 Average shear strength of single lap joints prepared with reference treatments.

Treatment	Average shear strength (MPa)	Shear strength standard deviation (MPa)
Untreated	2.68	0.36
Primer	3.40	0.24
Abrasion	4.60	0.32
Plasma	8.12	0.56

3.1.2 PL scanning strategy

The first set of experiments with the PL scanning strategy (Table 4) saw increases in average shear strength with increasing average laser power and decreasing hatch spacing and scanning velocity over the tested parameter range (Table 4). Highest average shear strength (11.04 MPa) was achieved with *P = 3* W, *h = 50* µm and *v* = 700 mm/s (*E* = 8.57 J/cm²). All data for this group are presented in Table 8 in the Appendix. These outcomes indicate that higher laser energy dose, achieved with higher pulse energy and greater pulse overlap, was beneficial to improving adhesion over the tested parameter range. Macroscopic melting was not observed on any of the laser-textured samples.

The ANOVA model equation for the first set of experiments with the PL scanning strategy was:

$$L = 14.4 + 0.44P - 0.072h - 4.8 \times 10^{-3}v + 4.4 \times 10^{-3}Ph + 4.0 \times 10^{-4}Pv + 2.5 \times 10^{-5}hv - 4.0 \times 10^{-6}Phv \quad (3)$$

where *L* is the shear strength (MPa), *P* the average laser power (W), *h* the hatch spacing (µm) and *v* the scanning velocity (mm/s). A full summary of ANOVA outcomes can be found in Table 12 in the Appendix.

Parameters leading to the highest average shear strength were subsequently chosen as the center point for the second set of experiments (Table 5). All data for this group are presented in Table 9 in the Appendix. Experimental data and ANOVA model surfaces are presented in Fig. 4. For values of hatch spacing ≤50 µm, consistently high shear strength was achieved with an average laser power of 3 W and a scanning velocity of 700 mm/s. Combinations of high power and low speed (higher energy dose), or low power and high speed (lower energy dose), instead led to a reduction in shear strength and larger dispersion. Very low scanning velocity (111 mm/s) led to poor joint strength due to the onset of macroscopic melting. Results were relatively invariable with hatch spacing for values less than or equal to 50 µm, while a decrease in average shear strength took place for higher values of hatch spacing as the separation distance between parallel laser passes exceeded the focused laser spot diameter (60 µm). These outcomes indicate that laser-texturing of PA 66 is much less sensitive to heat accumulation in the lateral (hatch) direction than the laser scanning direction due to the long time delay between adjacent laser pulses in the former case. This is clearly illustrated by the very large difference in average shear strength between the parameter combinations *P = 3* W, *h = 50* µm, *v* = 111 mm/s (3.92 MPa) and *P = 3* W, *h = 8* µm, *v* = 700 mm/s (11.64 MPa), which both employed the highest tested laser energy dose (53.87 J/cm²).

The ANOVA model equation for the second set of experiments with the PL scanning strategy was:

$$L = 10.7 + 1.11P + 0.029h - 3.7 \times 10^{-3}v - 2.0 \times 10^{-3}Ph + 1.6 \times 10^{-3}Pv + 4.2 \times 10^{-5}hv - 0.31P^2 - 7.9 \times 10^{-4}h^2 - 2.3 \times 10^{-6}v^2 \quad (4)$$

The model was considered valid for *v* > 300 mm/s, as data relating to lower values of scanning velocity were excluded due to large-scale melting and very low joint strength. A full summary of ANOVA outcomes can be found in Table 13 in the Appendix.

The acquired topography of laser-textured PA 66 substrates and photographs of the fracture surfaces are presented in Fig. 5 for *P = 3* W, *h = 50* µm, *v* = 111 mm/s and *P = 3* W, *h = 50* µm, *v* = 700 mm/s. In the former case, the resulting topography was characterized by a series of ridges separated by the hatch distance (50 µm), superimposed on larger-scale waviness. Clear indications of melting were visible to the naked eye, with the surface becoming more reflective. The maximum shear strength in this case was 3.92 MPa, indicating that surface melting was detrimental to adhesion despite modest improvements compared to primed joints. Fracture surfaces were characterized by interfacial failure, where clean separation between the adhesive and substrate took place. In the second case, the resulting topography was characterized by a series of irregular acute peaks resulting from partial ejection of molten material during laser exposure, superimposed on ridges separated by the hatch distance. The average shear strength in this case was 11.60 MPa, amongst the highest of all parameter combinations. Fracture surfaces were characterized by cohesive failure, where bonding between the adhesive and substrate was stronger than the adhesive itself. Fracture of the PA 66 plates also took place due to bending induced during failure of the adhesive. This phenomenon had been observed previously by Musiari and Moroni [12] via photography for the same substrate-adhesive combination.

Although an average shear strength of 11.64 MPa was achieved with a hatch spacing of 8 µm, the improvement over results achieved with a hatch spacing of 50 µm was less than the experimental error (standard deviation: 0.24 – 0.40 MPa) while the energy dose was several times higher, requiring much longer processing times. In view of industrial application, the parameter set *P = 3* W, *h = 50* µm, *v* = 700 mm/s was considered as optimum for subsequent fatigue tests.

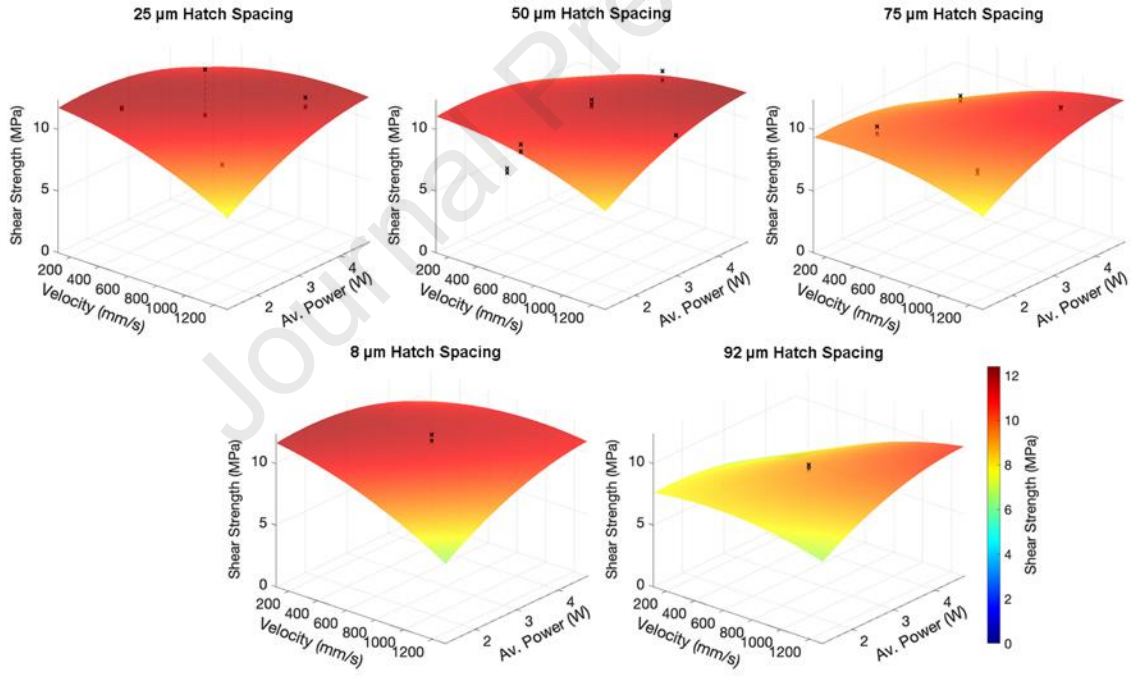

Fig. 4 Experimental data and ANOVA model surfaces for second set of experiments with PL strategy.

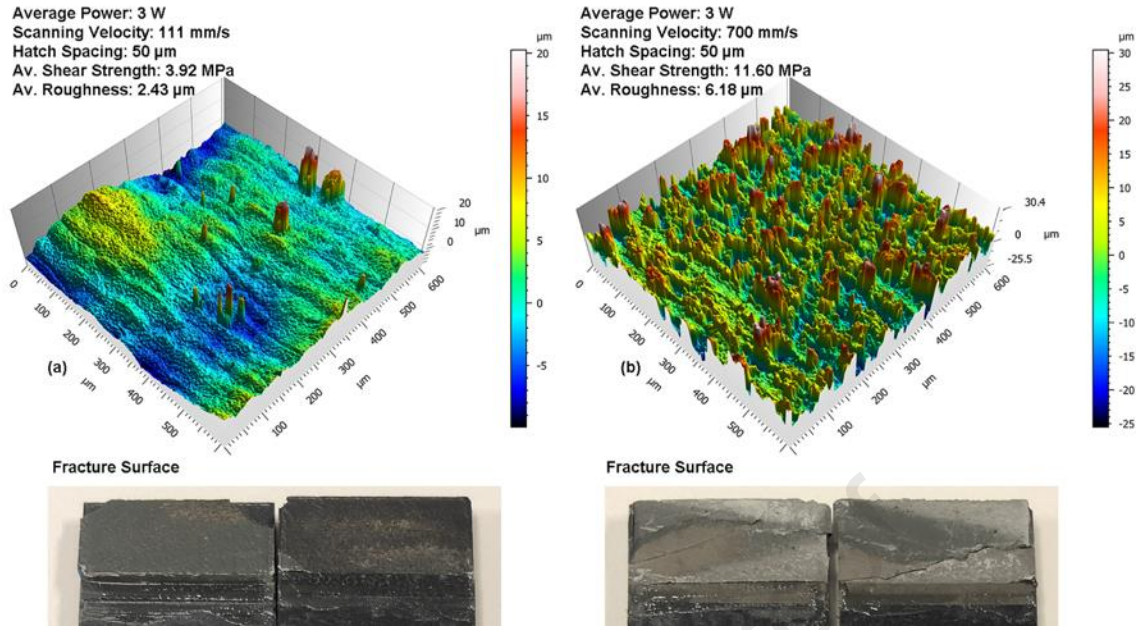

Fig. 5 Acquired topography of laser-textured PA 66 substrates and photographs of fracture surface for PL strategy: a) *P = 3* W, *h = 50* µm, *v* = 111 mm/s and b) *P = 3* W, *h = 50* µm, *v* = 700 mm/s

3.1.2 CL scanning strategy

The first set of experiments with the CL scanning strategy saw similar trends to the PL scanning strategy, with increases in average shear strength taking place with increasing average laser power and decreasing hatch spacing and scanning velocity over the tested parameter range (Table 4). Highest average shear strength (11.16 MPa) was achieved with *P = 3* W, *h = 50* µm and *v* = 700 mm/s (*E* = 17.14 J/cm²). All data for this group are presented in Table 10 in the Appendix. As with the PL scanning strategy, higher energy dose was associated with improvements in adhesion, while macroscopic melting effects were not observed on any of the surfaces.

The ANOVA model equation for the first set of experiments with the CL scanning strategy was:

$$L = 15.99 - 1.05P - 0.071h - 4.0 \times 10^{-3}v + 0.018Ph + 1.2 \times 10^{-3}Pv + 2.0 \times 10^{-5}hv - 1.0 \times 10^{-5}Phv \quad (5)$$

A full summary of ANOVA outcomes can be found in Table 14 in the Appendix. The center point of the second set of experiments (Table 5) was again chosen as parameters leading to the highest average shear strength in the first set of experiments. In the second set, joint strength was generally lower than for the PL scanning strategy, with greater variability. All data for this group are presented in Table 11 in the Appendix. Experimental data and ANOVA model surfaces are presented in Fig. 6. The CL scanning strategy only achieved a clear improvement in shear strength over the PL strategy with parameters leading to the lowest tested energy dose (*P = 2* W, *h = 75* µm, *v* = 1050 mm/s, *E* = 5.08 J/cm²), while in all other cases joint strength was similar or lower than the PL scanning strategy. These outcomes suggest that an additional laser pass with an angular offset of 90° provides no advantage for laser texturing of adhesive-bonded PA 66 joints where the energy dose is above approximately 5 J/cm².

The ANOVA model equation for the second set of experiments with the CL scanning strategy was:

$$L = 14.34 - 1.60P + 0.050h - 9.0 \times 10^{-3}v - 8.5 \times 10^{-3}Ph + 1.9 \times 10^{-4}Pv + 3.9 \times 10^{-5}hv + 0.28P^2 - 5.6 \times 10^{-4}h^2 + 4.6 \times 10^{-6}v^2 \quad (6)$$

The model was again considered valid for *v* > 300 mm/s, as data relating to lower values of scanning velocity were excluded due to the onset of macroscopic melting and very low joint strength. A full summary of ANOVA outcomes can be found in Table 15 in the Appendix.

The acquired topography of laser-textured PA 66 substrates and photographs of the fracture surfaces are presented in Fig. 7 for *P = 3* W, *h = 50* µm, *v* = 111 mm/s and *P = 3* W, *h = 50* µm, *v* = 1289 mm/s. In the former case, the surface was characterized by rounded surface features with no distinct periodicity. As with the PL scanning strategy, clear indications of melting were visible to the naked eye, with the surface becoming more reflective. The maximum shear strength was 3.44 MPa, indicating poor adhesion due to extensive melting. This was again confirmed by fracture surfaces characterized by interfacial failure. In the second case, the surface topography was characterized by a series of irregular acute peaks superimposed on a series of ridges separated by the hatch spacing (50 µm). The topography was somewhat similar to that achieved with the PL scanning strategy, as ridges resulting from the final laser pass were more evident than those resulting from the first. Nonetheless, the density of peaks was visibly higher due to the additional laser pass. The

average shear strength in this case was 11.40 MPa, indicating strong adhesion. As with the PL scanning strategy, fracture surfaces were characterized by cohesive failure, where fracture took place within the adhesive.

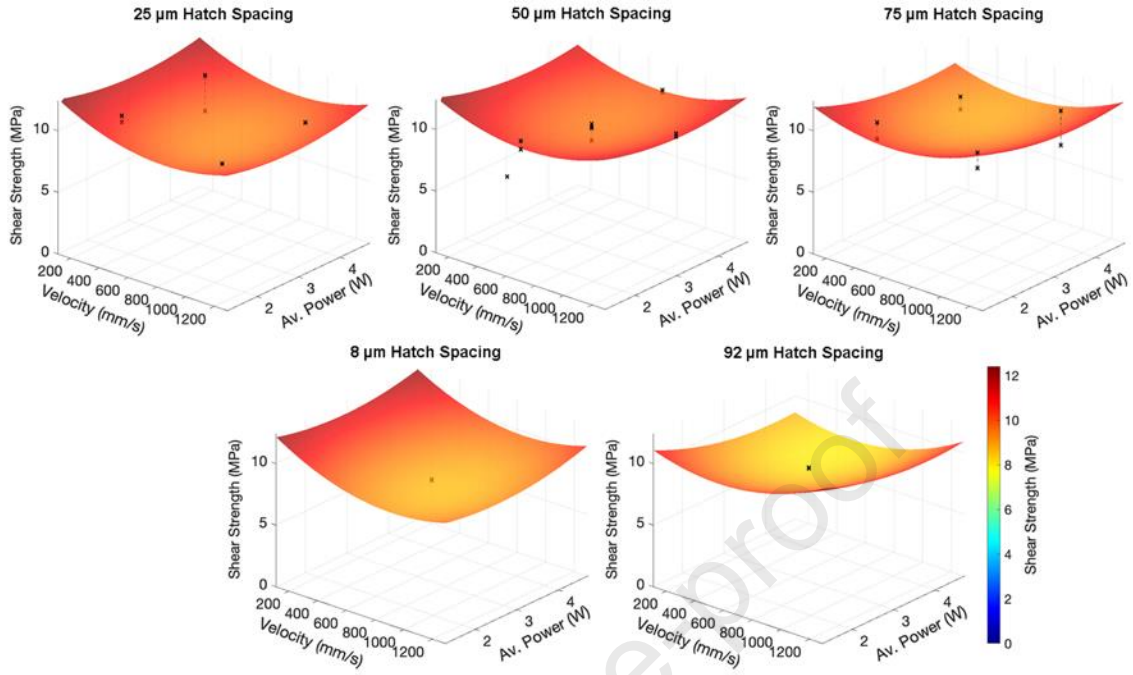

Fig. 6 Experimental data and ANOVA model surfaces for second set of experiments with CL strategy.

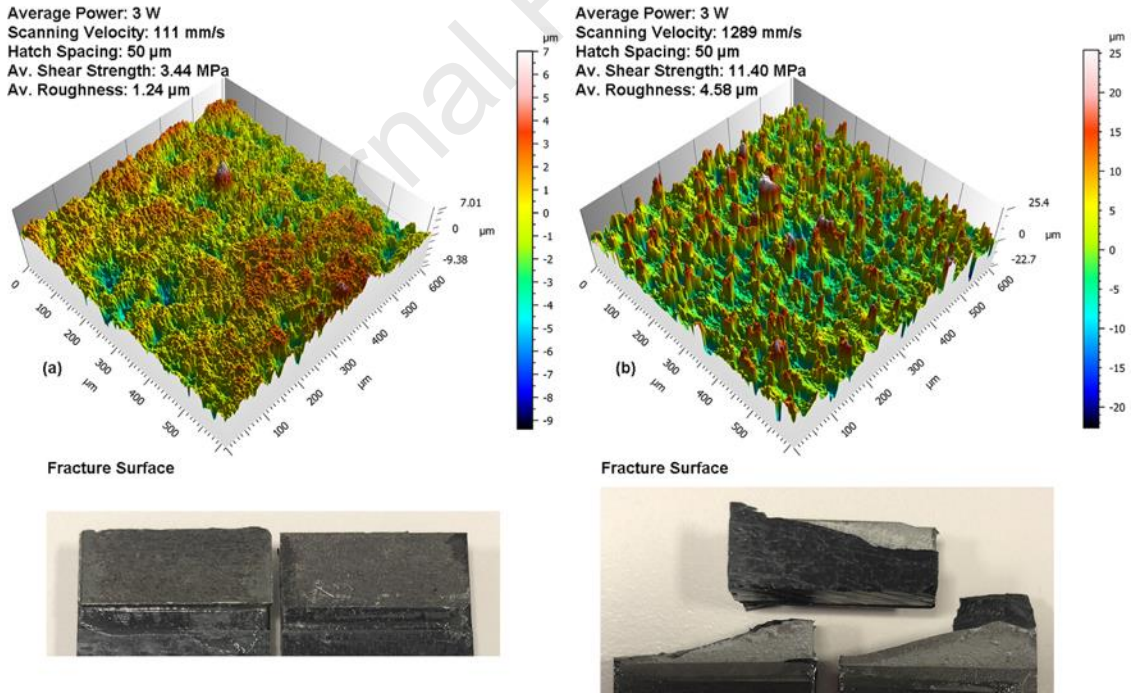

Fig. 7 Acquired topography of laser-textured PA 66 substrate and photographs of fracture surface for CL strategy: a) *P = 3* W, *h = 50* µm, *v* = 111 mm/s and b) *P = 3* W, *h = 50* µm, *v* = 1289 mm/s

3.2 Fatigue tests

Results of fatigue tests performed on PA 66 adhesive-bonded joints subject to primer, mechanical abrasion, plasma and laser treatments are presented in Fig. 8, where the maximum value of the applied average shear stress over the loading cycle is plotted against the number of cycles to failure. Joints treated with primer exhibited poor performance under cyclic loading, achieving 4.8×10^2 cycles with a maximum average cyclic shear stress of 1.89 MPa and $0.31\text{-}1.4\times10^6$ cycles with 1.22 MPa. Results achieved with mechanical abrasion

and plasma treatment instead allowed comparison of the relative influence of adhesion and microscale surface roughness on fatigue resistance. Mechanical abrasion achieved 1.7-7.3×10^3 cycles with a cyclic shear stress of 1.89 MPa and 0.78-1.1×10^6 cycles with 1.44 MPa. Plasma treatment achieved greater fatigue resistance at high cyclic shear stress, 6.1-9.7×10^3 cycles with 2.78 MPa, but poorer resistance at low cyclic shear stress, 0.32-1.1×10^6 cycles with 1.44 MPa. Plasma treatment induces chemical changes that greatly improve static joint strength and fatigue resistance at high cyclic shear stress; however, low microscale surface roughness leads to relatively poor performance at low cyclic shear stress as crack propagation is fast once this phase initiates. This outcome, together with the greater fatigue resistance of samples subject to mechanical abrasion at low cyclic shear stress, implies that adhesion is of greater importance to fatigue performance at high cyclic shear stress while microscale surface roughness is more influential at low cyclic shear stress.

Laser texturing clearly led to the best outcomes in terms of fatigue strength across the entire range of loading conditions, achieving 0.67-1.1×10^4 cycles with a maximum average cyclic shear stress of 3.22 MPa and 7.3×10^6 cycles with 1.67 MPa. These outcomes imply that laser texturing led to improved adhesion, resulting in high static strength and fatigue resistance at high cyclic shear stress, as well as impedance to crack propagation, resulting in high fatigue resistance at low cyclic shear stress. While the latter was likely associated with increased microscale surface roughness following laser irradiation (Fig. 3), the former may have been due to chemical changes taking place following laser irradiation. This aspect requires further investigation to determine the exact pathways leading to improved adhesion. Previous studies have shown that laser irradiation of PA6 and PA66 can lead to changes in FTIR and Raman spectra in relation to peaks corresponding to N-H stretching, C=O stretching, and CH_2 symmetric and asymmetric stretching. Such changes have been observed with pulsed and continuous-wave exposure by Koussi et al. [22] and Lim et al. [23], respectively, and were associated with improved adhesion in the latter case. Changes to functional groups have been observed following combined plasma/UV treatment by Weclawski et al. [24], as well as plasma treatment alone by Peng et al. [25] and Haji et al. [26], and were associated with improved adhesion by Musiari and Mororni [12].

Trends observed during fatigue tests were confirmed upon observation of the fracture surfaces shown in Fig. 9. It can be seen that surfaces treated with abrasion, primer and plasma yielded completely adhesive failure, with little or no residue of the adhesive on one of the two adherends. For these treatments, the crack initiated on one side of the overlap and then propagated to the other end, leading to complete failure of the joints. A different fracture surface can instead be seen for laser treatment. In most cases, a mixed-adhesive fracture was observed, meaning that two cracks initiated on both sides of the overlap and simultaneously grew towards the center of the specimens. This behavior yields greater joint resistance during the propagation phase, thus leading to a greater number of cycles to failure. These outcomes imply that nanosecond pulsed laser irradiation is an appropriate preparation method not only for improving resistance to static loads, but also for greatly increasing service life under cyclic conditions over a range of cyclic shear stresses.

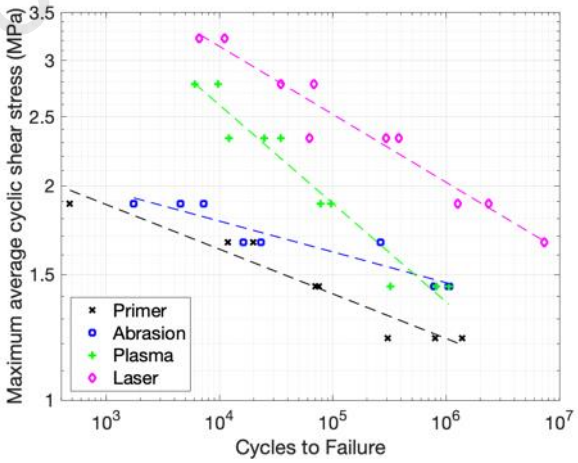

Fig. 8 Maximum average cyclic shear stress versus cycles to failure for PA 66 adhesive-bonded joints subject to various preparation methods.

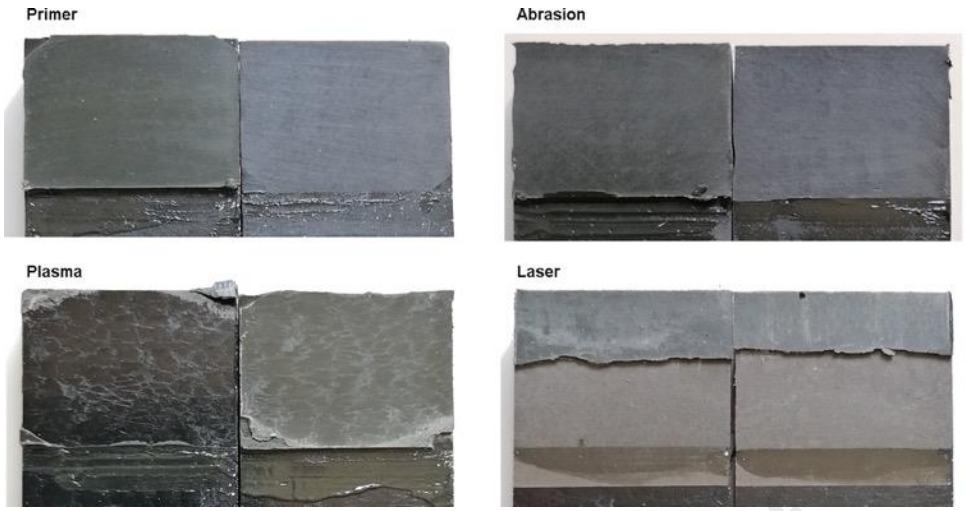

Fig. 9 Photographs of fatigue specimen fracture surfaces for PA 66 adhesive-bonded joints subject to various preparation methods.

4 CONCLUSION

With appropriate optimization, nanosecond pulsed laser irradiation is an effective preparation method for improving both the static and fatigue shear strength of PA 66 adhesive-bonded joints in a lap configuration. In the present case, a static average shear strength of 11.60 MPa was achieved with a parallel-line (PL) scanning strategy and an average laser power of 3 W, hatch spacing of 50 µm and scanning velocity of 700 mm/s. These parameters led to cohesive failure and a more than three-fold increase in shear strength compared to standard primed joints with the same geometry. Although marginally higher strength was achieved with a hatch spacing of 8 µm, the improvement over a hatch spacing of 50 µm was less than the experimental error while the energy dose and processing time were several times higher. In terms of fatigue strength, laser-textured PA 66 adhesive-bonded joints achieved 0.67-1.1×10^4 cycles with a maximum average cyclic shear stress of 3.22 MPa and 7.3×10^6 cycles with a cyclic shear stress of 1.67 MPa, significantly exceeding the performance of atmospheric pressure plasma, mechanical abrasion and primer treatments at both high and low cyclic shear stress.

Laser texturing of PA 66 was found to be far less sensitive to heat accumulation in the lateral (hatch) direction than the laser scanning direction due to the much longer time delay between successive pulses in the former case. As a result, the process was relatively insensitive to hatch spacing where complete surface coverage was achieved, while excessively low scanning speed was generally detrimental to joint strength due to the onset of macroscopic melting. An optimum energy dose of approximately 8-20 J/cm^2 could be achieved in a single laser pass with the PL strategy, for which use of a crossing-line (CL) scanning strategy was found to be of no advantage. These outcomes were fundamentally different to those observed for PE joints bonded with Teroson 9399 in a previous study by the authors, where the CL scanning was beneficial in achieving the optimum energy dose without onset of macroscopic melting. The observed differences between pigmented PA 66 and PE suggest that careful attention must be paid to optimization of laser parameters for individual polymer-adhesive combinations.

While the role of surface chemistry must now be investigated further, the lack of correlation between the surface microscale roughness and static joint strength for low values of the former (S_a < 2 µm), together with the high fatigue strength of laser-textured joints across all tested cyclic shear stresses, imply that laser irradiation achieved changes in both adhesion and morphology that were instrumental to improving joint performance over a range of cyclic shear stresses. Further investigation into the resulting topography on the nanoscale may also be beneficial to further understanding the observed outcomes. For the specific polymer-adhesive combination under consideration, changes in adhesion are likely to have played a role in increasing the static and fatigue strength at high cyclic shear stress due to improved bonding, while changes in microscale surface roughness are likely to have played a role in increasing the fatigue strength at low cyclic shear stress by prolonging the crack propagation phase. While the contribution of these aspects must now be studied in greater detail, nanosecond pulsed laser irradiation is a promising approach to improving the static and fatigue performance of polymer adhesive-bonded joints.

ACKNOWLEDGEMENTS

This research has been financially supported by the “FIL-Quota Incentivante” Program at the University of Parma, co-sponsored by Fondazione Cariparma.

REFERENCES

[1] Silva LRR, Marques EAS, da Silva LFM. Polymer joining techniques state of the art review. Welding in the World 2021. https://doi.org/10.1007/s40194-021-01143-x

[2] ASTM D2093 - 03(2017) Standard practice for preparation of surfaces of plastics prior to adhesive bonding. West Conshohocken: ASTM International; 2017.

[3] Ebnesajjad S. Surface treatment of materials for adhesive bonding. Oxford: William Andrew; 2014.

[4] Lutey AHA, Moroni F. Pulsed laser texturing for improved adhesive-bonded polyethylene (PE) joints. International Journal of Adhesion and Adhesives 2020;102:102676. https://doi.org/10.1016/j.ijadhadh.2020.102676

[5] Lippert T. Interaction of photons with polymers: From surface modification to ablation. Plasma Processes and Polymers 2005;2:525-46. https://doi.org/10.1002/ppap.200500036

[6] Kagan VA, Bray RG, Kuhn WP. Laser transmission welding of semi-crystalline thermoplastics-Part I: Optical characterization of nylon based plastics. Journal of Reinforced Plastics and Composites 2002;21:1101-22. https://doi.org/10.1177/073168402128987699

[7] Ravi-Kumar S, Lies B, Zhang X, Lyu H, Qin H. Laser ablation of polymers: A review. Polymer International 2019;68:1390-401. https://doi.org/10.1002/pi.5834

[8] Schäfer J, Hofmann T, Holtmannspötter J, Frauenhofer M, von Czarnecki J, Gudladt H-J. Atmospheric-pressure plasma treatment of polyamide 6 composites for bonding with polyurethane. Journal of Adhesion Science and Technology 2015;29:1807-19. https://doi.org/10.1080/01694243.2015.1037380

[9] Kłonica M, Kuczmaszewski J, Kwiatkowski MP, Ozonek J. Polyamide 6 surface layer following ozone treatment. International Journal of Adhesion & Adhesives 2016;64:179-87. https://doi.org/10.1016/j.ijadhadh.2015.10.017

[10] Mandolfino C, Lertora E, Gambaro C. Influence of cold plasma treatment parameters on the mechanical properties of polyamide homogeneous bonded joints. Surface & Coatings Technology 2017;313:222-9. https://doi.org/10.1016/j.surfcoat.2017.01.071

[11] Arikan E, Holtmannspötter J, Zimmer F, Hofmann T, Gudladt H-J. The role of chemical surface modification for structural adhesive bonding on polymers – Washability of chemical functionalization without reducing adhesion. International Journal of Adhesion and Adhesives 2019;95:102409. https://doi.org/10.1016/j.ijadhadh.2019.102409

[12] Musiari F, Moroni F. Experimental study of the influence of the surface preparation on the fatigue behavior of polyamide single lap joints. Materials 2021;14:1008. https://doi.org/10.3390/ma14041008

[13] Pappas D, Bujanda A, Demaree JD, Hirvonen JK, Kosik W, Jensen R, McKnight S. Surface modification of polyamide fibers and films using atmospheric plasmas. Surface & Coatings Technology 2006;201:4384-8. https://doi.org/10.1016/j.surfcoat.2006.08.068

[14] Quaresimin M, Ricotta M. Fatigue behaviour and damage evolution of single lap bonded joints in composite material. Composites Science and Technology 2006;66:176-87. https://doi.org/10.1016/j.compscitech.2005.04.026

[15] Shenoy V, Ashcroft IA, Critchlow GW, Crocombe AD, Abdel Wahab MM. An investigation into the crack initiation and propagation behaviour of bonded single-lap joints using backface strain. International Journal of Adhesion and Adhesives 2009;29:361-71. https://doi.org/10.1016/j.ijadhadh.2008.07.008

[16] ASTM D3163 - 01(2014) Standard test method for determining strength of adhesively bonded rigid plastic lap-shear joints in shear by tension loading. West Conshohocken: ASTM International; 2014.

[17] Montgomery DC, Runger GC. Applied statistics and probability for engineers. New York: John Wiley & Sons; 2011

[18] Anderson MJ, Whitcomb PJ, RSM Simplified: Optimizing Processes Using Response Surface Methods for Design of Experiments. Productivity Press 2016, ISBN 9781498745987

[19] ISO 25178-2:2012 Geometrical product specifications (GPS) – Surface texture: Areal – Part 2: Terms, definitions and surface texture parameters. Geneva: International Organization for Standardization; 2012.

[20] Moroni F, Musiari F, Sciancalepore C, Messori M. Influence of atmospheric pressure plasma process parameters on the mechanical behavior of thermoplastic joints. Int J Adhes Adhes 2020;102:102650. https://doi.org/10.1016/j.ijadhadh.2020.102650

[21] ASTM D3166 - 99(2020) Standard test method for fatigue properties of adhesives in shear by tension loading (metal/metal). West Conshohocken: ASTM International; 2020.

[22] Koussi E-K, Jung HJ, Faure N, Donnet C, Mauclair C, Sedao X, Comparative study of ultraviolet and infrared femtosecond laser irradiation on textile polymers PET and PA66. Journal of Laser Mirco / Nanoengineering 2020;15:245-51.

[23] Lim SJ, Cheon J, Kim M, Effect of laser surface treatments on a thermoplastic PA 6/carbon composite to enhance the bonding strength, Composites Part A 2020;137:105989. https://doi.org/10.1016/j.compositesa.2020.105989

[24] Weclawski BT, Horrocks AR, Ebdon JR, Mosurkal R, Kandola BK, Combined atmospheric pressure plasma and UV surface functionalization and diagnostics of nylon 6.6 fabrics, Applied Surface Science 2021;562:150090. https://doi.org/10.1016/j.apsusc.2021.150090

[25] Peng M, Li L, Xiong J, Hua K, Wang S, Shao T, Study on surface properties of polyamide 66 using atmospheric glow-like discharge plasma treatment, Coatings 2017;7:123. https://doi.org/10.3390/coatings7080123

[26] Haji A, Shoushtari AM, Mirafshar M, Natural dyeing and antibacterial activity of atmospheric-plasma-treated nylon 6 fabric, Coloration Technology 2013;130:37-42. https://doi.org/10.1111/cote.12060

APPENDIX

Table 8 Process parameters and static adhesive-bonded joint strength for set 1, PL scanning strategy.

Average power [W]	Scanning velocity [mm/s]	Hatch spacing [µm]	Laser energy dose [J/cm^2]	Average shear strength [MPa]	Shear strength standard deviation [MPa]
1	700	50	2.86	9.44	0.68
1	700	150	0.95	4.28	0.52
1	2100	50	0.95	4.80	1.56
1	2100	150	0.32	2.60	0.64
2	1400	100	1.43	5.40	0.60
3	700	50	8.57	11.04	1.00
3	700	150	2.86	6.24	0.48
3	2100	50	2.86	6.96	0.20
3	2100	150	0.95	3.96	0.44

Table 9 Process parameters and static adhesive-bonded joint strength for set 2, PL scanning strategy.

Average power [W]	Scanning velocity [mm/s]	Hatch spacing [µm]	Laser energy dose [J/cm^2]	Average shear strength [MPa]	Shear strength standard deviation [MPa]
1.3	700	50	3.77	10.76	0.44
2	350	25	22.86	11.52	0.08
2	350	75	7.62	9.72	0.44
2	1050	25	7.62	9.68	0.04
2	1050	75	2.54	9.08	0.20
3	111	50	53.87	3.92	0.24
3	700	8	53.87	11.64	0.40
3	700	50	8.57	11.60	0.24
3	700	92	4.66	9.28	0.24
3	1289	50	4.66	11.40	0.02
4	350	25	45.71	9.60	2.64
4	350	75	15.24	9.12	0.32
4	1050	25	15.24	11.52	0.56
4	1050	75	5.08	11.04	0.08
4.7	700	50	13.38	11.20	0.52

Table 10 Process parameters and static adhesive-bonded joint strength for set 1, CL scanning strategy.

Average power [W]	Scanning velocity [mm/s]	Hatch spacing [µm]	Laser energy dose [J/cm^2]	Average shear strength [MPa]	Shear strength standard deviation [MPa]
1	700	50	5.71	10.56	0.20
1	700	150	1.90	5.92	0.84
1	2100	50	1.90	7.28	0.56
1	2100	150	0.63	4.12	0.24
2	1400	100	2.86	8.32	0.56
3	700	50	17.14	11.16	0.24
3	700	150	5.71	8.64	1.52
3	2100	50	5.71	9.72	0.28
3	2100	150	1.90	5.88	0.36

Table 11 Process parameters and static adhesive-bonded joint strength for set 2, CL scanning strategy.

Average power [W]	Scanning velocity [mm/s]	Hatch spacing [µm]	Laser energy dose [J/cm^2]	Average shear strength [MPa]	Shear strength standard deviation [MPa]
1.3	700	50	7.53	11.00	0.48
2	350	25	45.71	10.76	0.40
2	350	75	15.24	9.80	0.96
2	1050	25	15.24	9.84	0.04
2	1050	75	5.08	10.12	0.88
3	111	50	107.75	3.44	0.004
3	700	8	107.75	8.24	0.08
3	700	50	17.14	9.52	0.60
3	700	92	9.31	9.20	0.04
3	1289	50	9.31	11.40	0.16
4	350	25	91.43	9.64	2.08
4	350	75	30.48	8.84	0.72
4	1050	25	30.48	10.00	0.04
4	1050	75	10.16	9.52	1.96
4.7	700	50	26.75	9.96	0.12

Table 12 ANOVA table [17] for the first set of experiments with the PL scanning strategy

Source	**Sum of Squares**	**Degrees of Freedom**	**Mean Square**	**F Value**	**p-value Prob > F**
Model	1.75×10^{2}	7	2.49×10^{1}	3.80×10^{1}	$< 1.00 \times 10^{-4}$
P-Average Power	1.89×10^{1}	1	1.89×10^{1}	2.89×10^{1}	$< 1.00 \times 10^{-4}$
h-Hatch Spacing	1.03×10^{1}	1	1.03×10^{1}	1.57×10^{1}	7.00×10^{-4}
v-Scan. Velocity	6.17×10^{0}	1	6.17×10^{0}	9.41×10^{0}	5.80×10^{-3}
Ph	8.21×10^{-2}	1	8.21×10^{-2}	1.25×10^{-1}	7.27×10^{-1}
Pv	4.17×10^{-4}	1	4.17×10^{-4}	6.36×10^{-4}	9.80×10^{-1}
hv	6.64×10^{-2}	1	6.64×10^{-2}	1.01×10^{-1}	7.53×10^{-1}
Phv	4.78×10^{-1}	1	4.78×10^{-1}	7.30×10^{-1}	4.03×10^{-1}
Residual	1.38×10^{1}	21	6.56×10^{-1}		
Lack of Fit	2.37×10^{0}	1	2.37×10^{0}	4.15×10^{0}	5.51×10^{-2}
Pure Error	1.14×10^{1}	20	5.70×10^{-1}		
Cor Total	1.88×10^{2}	28			

Table 13 ANOVA table for the second set of experiments with the PL scanning strategy

Source	Sum of Squares	Degrees of Freedom	Mean Square	F Value	p-value Prob > F
Model	2.61×10^{1}	9	2.90×10^{0}	1.59×10^{1}	$< 1.00 \times 10^{-4}$
P-Average Power	1.23×10^{0}	1	1.23×10^{0}	6.71×10^{0}	1.79×10^{-2}
h-Hatch Spacing	9.75×10^{-1}	1	9.75×10^{-1}	5.34×10^{0}	3.23×10^{-2}
v-Scan. Velocity	4.25×10^{0}	1	4.25×10^{0}	2.33×10^{1}	1.00×10^{-4}
Ph	3.65×10^{-2}	1	3.65×10^{-2}	2.00×10^{-1}	6.60×10^{-1}
Pv	4.71×10^{0}	1	4.71×10^{0}	2.58×10^{1}	$< 1.00 \times 10^{-4}$
hv	2.01×10^{0}	1	2.01×10^{0}	1.10×10^{1}	3.60×10^{-3}
P^2	1.73×10^{0}	1	1.73×10^{0}	9.45×10^{0}	6.20×10^{-3}
h^2	4.39×10^{0}	1	4.39×10^{0}	2.41×10^{1}	$< 1.00 \times 10^{-4}$
v^2	9.50×10^{-1}	1	9.50×10^{-1}	5.21×10^{0}	3.42×10^{-2}
Residual	3.47×10^{0}	19	1.83×10^{-1}		
Lack of Fit	1.97×10^{0}	4	4.93×10^{-1}	4.95×10^{0}	9.60×10^{-3}
Pure Error	1.50×10^{0}	15	9.97×10^{-2}		
Cor Total	2.96×10^{1}	28			

Table 14 ANOVA table for the first set of experiments with the CL scanning strategy

Source	Sum of Squares	Degrees of Freedom	Mean Square	F Value	p-value Prob > F
Model	1.32×10^{2}	7	1.89×10^{1}	4.22×10^{1}	$< 1.00 \times 10^{-4}$
P-Average Power	2.13×10^{1}	1	2.13×10^{1}	4.77×10^{1}	$< 1.00 \times 10^{-4}$
h-Hatch Spacing	3.54×10^{0}	1	3.54×10^{0}	7.92×10^{0}	1.04×10^{-2}
v-Scan. Velocity	1.59×10^{0}	1	1.59×10^{0}	3.56×10^{0}	7.30×10^{-2}
Ph	7.95×10^{-1}	1	7.95×10^{-1}	1.78×10^{0}	1.97×10^{-1}
Pv	3.16×10^{-1}	1	3.16×10^{-1}	7.06×10^{-1}	4.10×10^{-1}
hv	2.56×10^{0}	1	2.56×10^{0}	5.73×10^{0}	2.61×10^{-2}
Phv	2.93×10^{0}	1	2.93×10^{0}	6.57×10^{0}	1.82×10^{-2}
Residual	9.39×10^{0}	21	4.47×10^{-1}		
Lack of Fit	7.49×10^{-1}	1	7.49×10^{-1}	1.73×10^{0}	2.03×10^{-1}
Pure Error	8.64×10^{0}	20	4.32×10^{-1}		
Cor Total	1.41×10^{2}	28			

Table 15 ANOVA table for the second set of experiments with the CL scanning strategy

Source	Sum of Squares	Degrees of Freedom	Mean Square	F Value	p-value Prob > F
Model	1.57×10^{1}	9	1.74×10^{0}	2.88×10^{0}	2.51×10^{-2}
P-Average Power	1.00×10^{0}	1	1.00×10^{0}	1.66×10^{0}	2.14×10^{-1}
h-Hatch Spacing	8.16×10^{-1}	1	8.16×10^{-1}	1.35×10^{0}	2.60×10^{-1}
v-Scan. Velocity	4.08×10^{-2}	1	4.08×10^{-2}	6.74×10^{-2}	7.98×10^{-1}
Ph	6.62×10^{-1}	1	6.62×10^{-1}	1.10×10^{0}	3.08×10^{-1}
Pv	6.14×10^{-2}	1	6.14×10^{-2}	1.02×10^{-1}	7.54×10^{-1}
hv	1.69×10^{0}	1	1.69×10^{0}	2.79×10^{0}	1.11×10^{-1}
P^2	1.37×10^{0}	1	1.37×10^{0}	2.27×10^{0}	1.48×10^{-1}
h^2	2.13×10^{0}	1	2.13×10^{0}	3.53×10^{0}	7.59×10^{-2}
v^2	3.93×10^{0}	1	3.93×10^{0}	6.50×10^{0}	1.96×10^{-2}
Residual	1.15×10^{1}	19	6.05×10^{-1}		
Lack of Fit	3.87×10^{0}	4	9.66×10^{-1}	1.90×10^{0}	1.63×10^{-1}
Pure Error	7.62×10^{0}	15	5.08×10^{-1}		
Cor Total	2.71×10^{1}	28			